



## Article

# Periodic Steady State Assessment of Microgrids with Photovoltaic Generation Using Limit Cycle Extrapolation and Cubic Splines

Marcolino Díaz-Araujo <sup>1</sup>, Aurelio Medina <sup>1,\*</sup>, Rafael Cisneros-Magaña <sup>1</sup>  and Amner Ramírez <sup>2</sup> 

<sup>1</sup> División de Estudios de Posgrado, Facultad de Ingeniería Eléctrica, Universidad Michoacana de San Nicolás de Hidalgo, Morelia 58030, México; geniusmhda@hotmail.com (M.D.-A.); rcisneros@dep.fie.umich.mx (R.C.-M.)

<sup>2</sup> Centro de Investigación y de Estudios Avanzados del Instituto Politécnico Nacional, Zapopan 45019, México; abner.ramirez@cinvestav.mx

\* Correspondence: amedinr@gmail.com; Tel.: +52-443-327-9728

Received: 14 June 2018; Accepted: 17 July 2018; Published: 13 August 2018



**Abstract:** This paper proposes a fast and accurate time domain (TD) methodology for the assessment of the dynamic and periodic steady state operation of microgrids with photovoltaic (PV) energy sources. The proposed methodology uses the trapezoidal rule (TR) technique to integrate the set of first-order differential algebraic equations (DAE), generated by the entire electrical system. The Numerical Differentiation (ND) method is used to significantly speed-up the process of convergence of the state variables to the limit cycle with the fewest number of possible time steps per cycle. After that, the cubic spline interpolation (CSI) algorithm is used to reconstruct the steady state waveform obtained from the ND method and to increase the efficiency of the conventional TR method. This curve-fitting algorithm is used only once at the end part of the algorithm. The ND-CSI can be used to assess stability, power quality, dynamic and periodic steady state operation, fault and transient conditions, among other issues, of microgrids with PV sources. The results are successfully validated through direct comparison against those obtained with the PSCAD/EMTDC simulator, widely accepted by the power industry.

**Keywords:** time domain; photovoltaic energy sources; periodic steady state; limit cycle; numerical differentiation method; cubic splines

## 1. Introduction

Renewable photovoltaic (PV) generation systems represent an attractive and viable alternative of electrical energy supply to decrease the environmental contamination and the global warming effect produced by the consumption of fossil fuels. The PV installations have been steadily growing over recent decades. At present, a considerable number of PV generation plants are connected to power networks or to supply isolated electrical loads [1].

The dynamic performance of these PV generation systems is important for the planning, design, and operation of power networks where they are connected [2,3]. This work mainly focuses in a time domain (TD) framework for the representation of these interconnected PV generation system working under dynamic and periodic steady state operation conditions [4].

Reported technical problems and limitations of PV generation are its variability, intermittency, and adverse power quality effects, such as harmonic distortion, voltage, and frequency variations [5]. These problems can be analysed with the proposed TD methodology. The TD solution can be applied

to take adequate control decisions, e.g., to regulate the power generation and the energy conversion process or to enhance the electrical network stability [6–8].

The extrapolation to the limit cycle and Poincare map approach [9] has been applied to quickly obtain the periodic steady state of electrical systems [10,11]. The proposed methodology extends this application to interconnected microgrids with PV sources, taking into account the energy conversion system through power electronic components, such as transistors, MOSFETs and IGBTs. This conversion process requires the commutation of these electronic devices at an adjustable or controllable frequency and needs an adequate time step during the TD solution process [12]. Among the several methods reported in [9], the Numerical Differentiation (ND) approach is known to have a relatively simple formulation and good precision characteristics. Besides, the ND method is numerically robust and it has good convergence properties [13]. Therefore, in this contribution, it is used to speed-up the periodic steady state solution of the microgrid with interconnected PV generation, and to reduce the execution time and the computational effort required to obtain the periodic steady state solution in TD.

The cubic spline interpolation (CSI) is a technique that has been applied to accurately estimate a new point between known data with smaller error than the obtained by using square or linear interpolation [14,15]. The application of the cubic splines is proposed to adjust the number of points per cycle needed to represent the periodic steady state waveform. The CSI approach enhances the ND response with a time step reduction, thus avoiding a large computational effort. The CSI technique obtains new solution points, adjusted with a smaller error.

This contribution presents an efficient TD solution process to obtain the periodic steady state of microgrids with PV generation sources. This process incorporates fast and precise mathematical and numerical tools such as Newton Raphson (NR), trapezoidal rule (TR), DN, and CSI, respectively. The proposed TD methodology can be used to assess stability [16,17], power quality [18–20], dynamic and periodic steady state operation, fault and transient conditions, among other issues, of microgrids with PV sources [21].

The rest of the paper is organized as follows: Section 2 deals with the microgrid description, its modelling and the interconnection of PV systems; Section 3 reviews the ND method based on the Poincare map and the extrapolation to the limit cycle concepts; Section 4 explains the CSI method to adjust the number of time steps per cycle and to define the time step to be used during the electrical system solution; Section 5 details a flowchart of the solution procedure; Section 6 reports the practical application of the methodology through a test case and limitations of the microgrid modelling; Section 7 draws the main conclusions of this research work.

## 2. System Description and Modelling

Figure 1 shows the configuration of a single-phase grid-connected PV generation system. It contains a PV array, a capacitor link, a DC/DC converter, a DC/AC converter, a filter, and a utility grid [12].

The capacitor link is connected to the output of the PV array to decouple the AC-system dynamics from the PV array. The DC/DC converter is used to maintain an adequate voltage level and for maximum power point tracking (MPPT) of the generation system [22]. The DC/AC converter is used to obtain AC power. Finally, the filter is used to mitigate the total harmonic distortion (THD) at the point of common coupling (PCC).

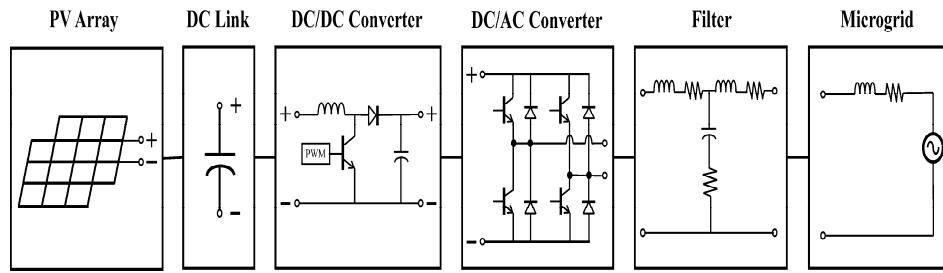


Figure 1. Single-phase grid-connected photovoltaic (PV) generation system.

### 2.1. PV Array Model

Typically, a single PV cell generates an electrical power of about 1 to 3 W [23]. To increase the power, several PV cells are connected in the appropriate series-parallel combination to form larger capacity units, called PV modules. Figure 2 shows the equivalent circuit of a practical PV module.

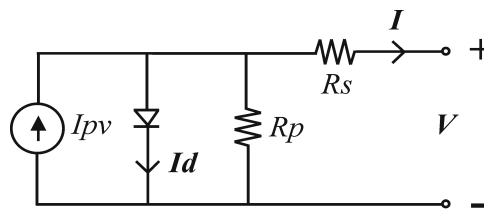


Figure 2. Single-diode model of the equivalent circuit of a practical PV module.

The equation from the theory of semiconductors that mathematically describes the characteristic of a practical PV module is [24,25]:

$$I = I_{pv} - I_0 \left[ \exp\left(\frac{V + R_s I}{a V_T}\right) - 1 \right] - \frac{V + R_s I}{R_p} \quad (1)$$

where  $I_{pv}$  and  $I_0$  are the generated PV and saturation currents of the PV module, respectively.  $I_d$  is the Shockley diode equation, which is the second term in (1).  $V_T = n_s k T_j / q$  is the thermal voltage of the module with  $n_s$  cells connected in series,  $q$  is the electron charge ( $1.60217646 \times 10^{-23}$  J/K), and  $T_j$  is the temperature on the p-n junction (Kelvin). In (1),  $a$  is the diode ideal constant,  $R_s$  is the equivalent series resistance of the PV module ( $\Omega$ ), and  $R_p$  is the equivalent parallel resistance ( $\Omega$ ).

From (1) the I-V curve can be obtained, where three particular points are highlighted, i.e., short circuit ( $0, I_{sc}$ ), maximum power point ( $V_{mpp}, I_{mpp}$ ), and open circuit ( $V_{oc}, 0$ ) [26]. This curve makes easier the adjustment and the validation of the desired mathematical I-V equation. Furthermore, it can help to determine the stability of the system, i.e., there can be potential instabilities within a grid-connected PV generation system if the operating point of the PV array is moved towards the constant region of the characteristic curve of a PV array [27]. Additionally, the P-V curve also dictates the performance of a PV module.

A PV array consists of  $N_p$  parallel and/or  $N_s$  series connected modules. To include a PV array model in the PV generation system, a Thevenin equivalent is obtained in this work based on the calculation of the  $R_p$  and  $R_s$  parameters of the model of Figure 2. Basically, this is achieved by solving the nonlinear relation (1), considering the PV array working at MPP.

The calculation of the PV Thevenin equivalent follows the steps detailed next:

**Step 1.** When a PV array is assembled,  $V_{oc}$  and  $I_{sc}$  are proportional to the number of series and parallel connected modules, respectively [23,26]. The total PV array characteristics are calculated with:

$$\begin{aligned}
V_{OC} &= N_s V_{oc} \\
V_{MPP} &= N_s V_{mpp} \\
I_{SC} &= N_p I_{sc} \\
I_{MPP} &= N_p I_{mpp}
\end{aligned} \tag{2}$$

Step 2. We assume that  $I_{pv}$  of the adopted model equates the maximum possible generated current ( $I_{sc}$ ). This permits to calculate  $I_0$  by using:

$$I_0 = \frac{I_{SC}}{\exp^{\frac{V_{OC}}{aV_T}} - 1} \tag{3}$$

Step 3. By considering that the PV array works at MPP, we evaluate (1) at the MPP, obtaining:

$$I_{MPP} = I_{PV} - I_0 \left[ \exp^{\left( \frac{V_{MPP} + R_S I_{MPP}}{aV_T} \right)} - 1 \right] - \frac{V_{MPP} + R_S I_{MPP}}{R_P} \tag{4}$$

Also, from Figure 3b it can be noticed that the derivative of the power with respect to the voltage is zero at the MPP. This condition is described by:

$$\frac{I_{MPP} R_S - V_{MPP}}{aV_T} I_0 \exp^{\frac{V_{MPP} + I_{MPP} R_S}{aV_T}} + I_{MPP} \left( \frac{R_S}{R_P} + 1 \right) - \frac{V_{MPP}}{R_S} = 0. \tag{5}$$

Thus, (4) and (5) are solved simultaneously in order to obtain  $R_S$  and  $R_P$ , for instance by using the Newton Raphson (NR) method.

Step 4. Once  $R_S$  and  $R_P$  are known from the solution of (4) and (5), and following the Thevenin theorem, the equivalent voltage source is obtained as:

$$V_{TH} = R_P \left[ I_{PV} - I_0 \left( \exp^{\frac{V_{MPP} + I_{MPP} R_S}{aV_T}} - 1 \right) \right] \tag{6}$$

and the equivalent resistance is given by:

$$R_{TH} = R_P + R_S. \tag{7}$$

The resultant Thevenin equivalent given by (6) and (7) is finally ready to be interfaced with the rest of the components and the grid.

## 2.2. DC/DC Converter

The DC/DC converter corresponds to the boost converter (BC). The main task of a BC is to maintain the output voltage  $v_{out}$  at a desired level, considering that the input voltage  $v_{in}$  and load may fluctuate. In the BC, the output voltage is always higher than the input voltage. When the switch is “on”, the diode is reverse biased, thus isolating the output stage. The input supplies energy to the inductor. When the switch is “off”, the output stage receives energy from the inductor as well as from the input. The switch is controlled by a pulse-width modulation (PWM) scheme in which the duty ratio  $d$ , defined as  $d = T_{on}/T_s$ , is adjusted as required [28];  $T_s$  represents the BC switching period, defined as the inverse of the switching frequency  $F_s$ , normally set at several kHz [29];  $T_{on}$  is the time in which the switch remains in “on” state within a switching period. The conduction time of the diode complements the conduction time of the switch.

For the PV generation system, it is desired that the PV array work at MPP;  $v_{in}$  of the BC (equal to the output voltage of the PV array) must be equated to  $V_{MPP}$  by adjusting  $d$ . Since the PV array depends on environmental conditions,  $V_{MPP}$  is variable. There are several MPPT algorithms; the most popular are the perturb and observe (P&O) and the incremental conductance (InC) methods [30]. Since this contribution ultimately focuses on the periodic steady state operation condition, it is assumed that the PV array works at the MPP by adopting the P&O method. Furthermore, the PV system is a non-feedback system, i.e., the output of the system has no influence or effect on the control action of the input signal. In other words, it is an open-loop system.

### 2.3. DC/AC Converter

Figure 3 shows a DC/AC converter. The main objective of a DC/AC converter is to generate a sinusoidal AC output voltage, whose magnitude and frequency can both be controlled. It can be observed from Figure 3 that the DC/AC converter corresponds to a single-phase full-bridge inverter. The switching actions of the inverter are controlled by a PWM scheme with unipolar voltage switching [28].

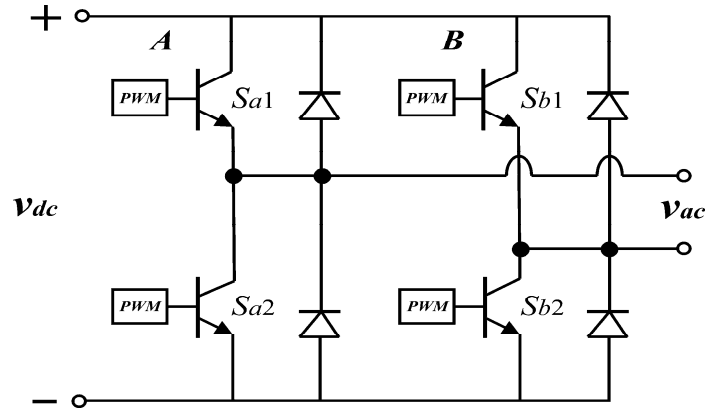


Figure 3. Single-phase full-bridge inverter.

Here, the switches in the legs A and B of the full-bridge inverter are controlled separately by comparing the triangular waveform  $V_{tri}$  (which establishes the switching frequency of the inverter switches) with two sinusoidal signals  $V_{control}$  and  $-V_{control}$  (which set the desired fundamental frequency of the inverter output voltage) as shown in Figure 4, where the peak value of  $V_{control}$  (the same for  $-V_{control}$ ) is related to  $V_{tri}$  through the modulation ratio  $m_a = V_{control}/V_{tri}$ .

It is observed that  $m_a$  corresponds also to the ratio between the magnitude of the fundamental component of the output voltage  $v_{ac}$  and the magnitude of the input voltage  $v_{dc}$ . The frequency of  $V_{tri}$  is fixed at several kHz, and determines the order of the harmonics of  $v_{ac}$  [28]. Harmonics in  $v_{ac}$  appear as sidebands centered at every two times the frequency modulation ratio  $m_f = f_s/f_0$ , where  $f_s$  is the switching frequency and  $f_0$  is the ac-system frequency.

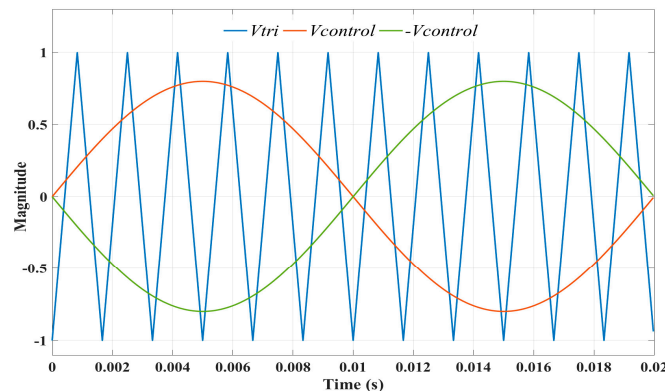


Figure 4. Sinusoidal pulse-width modulation (PWM) for unipolar voltage switching.

In the unipolar PWM voltage switching scheme applied to the inverter, the control for leg A is independent of the control of leg B. For leg A, when  $V_{control} < V_{tri}$ ,  $S_{a1}$  is turned on, otherwise is turned off ( $S_{a2}$  is always complementary to  $S_{a1}$ ). The same rule governs the control of leg B, but using  $-V_{control}$  instead of  $V_{control}$ .

### 3. Efficient Time-Domain Solution Using the Numerical Differentiation Method

The ND method can be applied to efficiently obtain the periodic steady state of a microgrid with PV energy sources. In principle, a nonlinear power network/component can be mathematically modelled by a set of first-order differential algebraic equations (DAEs), and using some integration routine, such as the TR or Fourth-Order Runge-Kutta (RK4) algorithm [31], the periodic steady state solution is obtained. This conventional process, known as “brute force” (BF) approach [9,32] can be inefficient, as it may require of a considerable time and computer effort. However, TD solution can be significantly accelerated to obtain the periodic steady state solution with the use of Newton type methods [10,13]. The mathematical model of DAEs is represented by state space equation:

$$\frac{dx}{dt} = [A]x + [B]u. \quad (8)$$

The extrapolation to the limit cycle of the state vector represented by  $x^\infty$  can be calculated as in [10], i.e.,

$$x^\infty = x^i + C(x^{i+1} - x^i) \quad (9)$$

$$C = (I - \Phi)^{-1} \quad (10)$$

$$\Phi = \frac{\partial x(t+T)}{\partial x(t)}. \quad (11)$$

where  $x^i$  is the state vector at the beginning of the base cycle,  $x^{i+1}$  is the state vector at the end of the base cycle,  $C$  is the iteration matrix,  $\Phi$  is the state transition matrix,  $I$  is the unit matrix,  $T$  is the fundamental frequency period.

The  $\Phi$  matrix can be approximated using finite-difference derivative as:

$$\Phi \approx \frac{\Delta x(t+T)}{\Delta x(t)}. \quad (12)$$

The identification of  $\Phi$  is detailed as follows: a base cycle  $x(t)$  is obtained through the numerical integration of (8) using the BF method during a defined number of cycles, depending of the system damping [10], and starting from a determined initial condition (e.g., zero condition). Usually, the number of cycles comprises the initial transient. A base cycle can be seen as the last cycle of this initial transient period. Then, the base cycle is sequentially perturbed with a small value at the beginning of the cycle for each state variable. The difference between the base cycle and the perturbed base cycle at the end of the cycle is then evaluated to obtain  $\Delta x^{i+1} = x^{i+1} - x^i$  for all the state variables. This allows the sequential identification of the state transition matrix by columns.

With  $\Phi$  identified, the iteration matrix  $C$  can be evaluated using (10). Finally, at this point the state vector at the limit cycle can be evaluated using (9). It represents the limit cycle estimation of the state vector. In other words, ND computes  $\Phi$  using a column-by-column process. The  $k$ th column of  $\Phi$  is  $\Phi_k$ , for  $k = 1, 2, \dots, n$ . This column can be computed by perturbing the  $k$ th state, i.e., let  $x(t) \rightarrow x(t) + \Delta x_k(t)$  and compute  $x(t+T) + \Delta x_k(t+T)$  by numerical integration of (8) over one period. By letting  $\Delta x_k(t)$  to be equal to  $\varepsilon U_k$ , with  $\varepsilon$  being a small real number, e.g.,  $10^{-6}$ , and  $U_k$  the  $k$ th column of a identity matrix of dimension  $n$ , for  $k = 1, 2, \dots, n$ , then, by considering (12) we obtain:

$$\Delta x_k(t+T) = \Phi \varepsilon U_k \quad (13)$$

and consequently

$$\Delta x_k(t+T) = \varepsilon \Phi_k. \quad (14)$$

Therefore

$$\Phi_k = \Delta x_k(t+T) / \varepsilon. \quad (15)$$

Each column of  $\Phi$  can be computed with (15). All  $n$  states of the system (8) must be perturbed separately in order to compute the  $n$  columns of the sensitivity matrix. Note that  $n + 1$  cycles must be computed to apply (9).

#### Variants of Solution

Different implementation strategies can be explored for the efficient solution of the microgrid with PV energy sources using the ND method. The identification of the  $\Phi$  matrix is the most computationally demanding task during the iterative TD location of the limit cycle. If  $\Phi$  and  $C$  are updated at each iteration step using (10) and (11), a Newton process of quadratic convergence to the limit cycle of the state variables results [10]. On the other hand, it becomes a linearly convergent process if  $\Phi$  and  $C$  are kept constant after the first evaluation using (10) and (11). However, this solution process is expected to be significantly faster than the first approach, since a repetitive identification of  $\Phi$  is avoided.

#### 4. Cubic Spline Interpolation

Once the ND method has obtained the steady state solution using the fewest number of data points, it does not represent the final solution and different order harmonics may appear. To avoid this, it is necessary to use an interpolation method to estimate intermediate data points using a mathematical function that minimizes the overall surface curvature, resulting in a surface that passes exactly through the input points. In this work, CSI is used. The objective of the CSI process is to derive a third-order polynomial for each interval of data points [14]. The polynomial for each interval can be represented by its general form:

$$f_i(x) = a_i x^3 + b_i x^2 + c_i x + d_i. \quad (16)$$

Figure 5 helps to explain the notation used to derive cubic splines. The first step in the derivation [33] is based on the observation that since each pair of knots is connected by a cubic function, the second derivative within each interval is a straight line. Equation (16) can be differentiated twice to verify this observation. On this basis, the second derivatives can be represented by a first-order Lagrange interpolating polynomial as:

$$f''_i(x) = f''_i(x_{i-1}) \frac{(x - x_i)}{(x_{i-1} - x_i)} + f''_i(x_i) \frac{(x - x_{i-1})}{(x_i - x_{i-1})} \quad (17)$$

where  $f''_i(x)$  is the value of the second derivative at any point  $x$  within the  $i$ th interval. Thus, this equation is a straight line connecting the second derivative at the first knot  $f''(x_{i-1})$  with the second derivative at the second knot  $f''(x_i)$ .

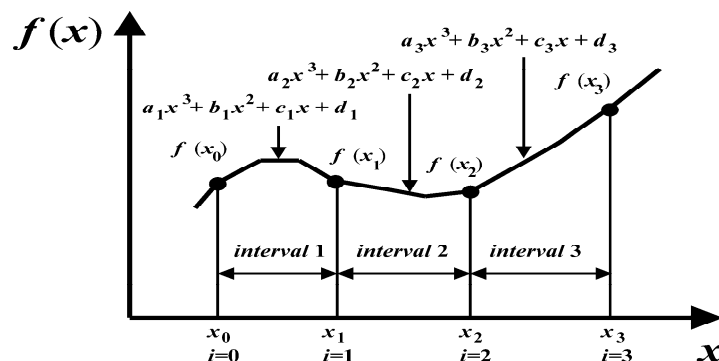


Figure 5. Notation used to derive cubic splines.

Next, (17) can be integrated twice to obtain an expression for  $f_i(x)$ . However, this expression will contain two unknown constants of integration. These constants can be evaluated by invoking the



function-equality conditions, i.e.,  $f(x)$  must equal to  $f(x_{i-1})$  at  $x_{i-1}$  and  $f(x)$  must equal to  $f(x_i)$  at  $x_i$ . By carrying out these evaluations, the following equation results:

$$f_i(x) = \frac{f''_i(x_{i-1})}{6(x_i - x_{i-1})}(x_i - x)^3 + \frac{f''_i(x_i)}{6(x_i - x_{i-1})}(x - x_{i-1})^3 + \left[ \frac{f(x_{i-1})}{(x_i - x_{i-1})} - \frac{f''_i(x_{i-1})(x_i - x_{i-1})}{6} \right](x_i - x) + \left[ \frac{f(x_i)}{(x_i - x_{i-1})} - \frac{f''_i(x_i)(x_i - x_{i-1})}{6} \right](x - x_{i-1}). \quad (18)$$

Clearly, this relationship is a much more complicated expression for the cubic spline for the  $i$ th interval than, say, (16). However, please notice that it has only two unknown coefficients, i.e., the second derivatives at the beginning and at the end of the interval  $f''(x_{i-1})$  and  $f''(x_i)$ . Thus, if we can define the proper second derivative at each knot, (18) is a third-order polynomial that can be used to interpolate within the interval.

The second derivatives can be evaluated by invoking the condition that the first derivatives at the knots must be continuous, i.e.,

$$f'_i(x_i) = f'_{i+1}(x_i). \quad (19)$$

Equation (18) can be differentiated to give an expression for the first derivative. If this is done for both, the  $(i - 1)$ th and the  $i$ th intervals, and the two results are set equal according to (19), the following relationship results:

$$(x_i - x_{i-1})f''(x_{i-1}) + 2(x_{i+1} - x_{i-1})f''(x_i) + (x_{i+1} - x_i)f''(x_{i+1}) = \frac{6}{(x_{i+1} - x_i)}[f(x_{i+1}) - f(x_i)] + \frac{6}{(x_i - x_{i-1})}[f(x_{i-1}) - f(x_i)] \quad (20)$$

If (20) is written for all interior knots,  $n - 1$  simultaneous equations result with  $n + 1$  unknown second derivatives. However, since this is a natural cubic spline, the second derivatives at the end knots are zero and the problem is reduced to  $n - 1$  equations with  $n - 1$  unknowns. In addition, notice that the system of equations will be tridiagonal. Thus, not only we have reduced the number of equations but we have also arranged them in a form that is extremely easy to solve.

## 5. General Time-Domain Solution Scheme

The flowchart of the time domain solution method to obtain the periodic steady state of microgrids with PV energy sources is shown in Figure 6.

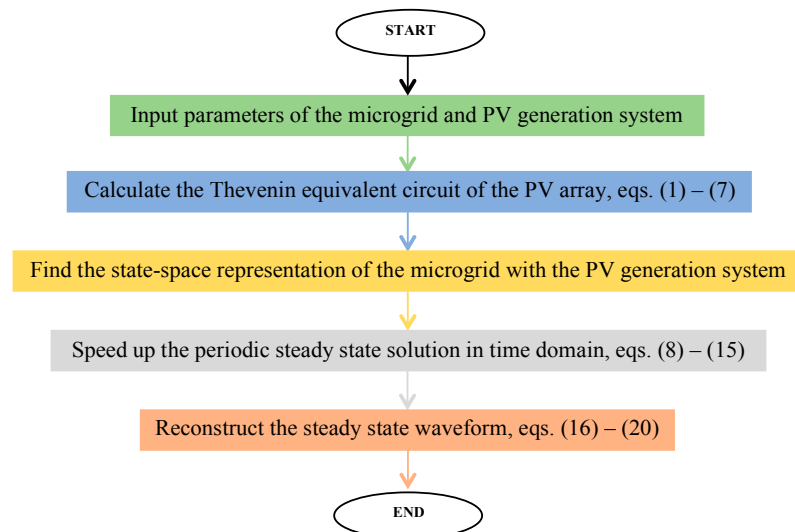


**Figure 6.** Flowchart of the Numerical differentiation method combined with cubic spline interpolation (ND-CSI) method.



It is basically composed by five blocks, whose function are as follows: the first block reads the parameters of the microgrid and the PV generation system, the second block obtains the Thevenin equivalent circuit of the PV array, the third block is based on the circuit of Figure 1, where the PV array is replaced by the corresponding Thevenin equivalent, finds the set of DAEs. In the fourth block, the DAE representation of the grid connected PV generation system is efficiently solved with the ND method. Finally, the fifth block reconstructs the steady state waveform using the CSI method.

## 6. Test Case

The periodic steady state solution of the single-phase grid-connected PV generation system of Figure 7 is obtained in the TD framework. The solution is obtained using the BF and ND combined with CSI methods. For the first case, the BF procedure is evaluated with a sampling time-step of  $0.1 \mu s$ . For the second case, ND obtains the periodic steady state with a sampling time-step of  $2.5 \mu s$ . Then, the CSI procedure is used just once to reconstruct the waveform. The criterion for convergence of the state variables has been set to  $10^{-4}$ .

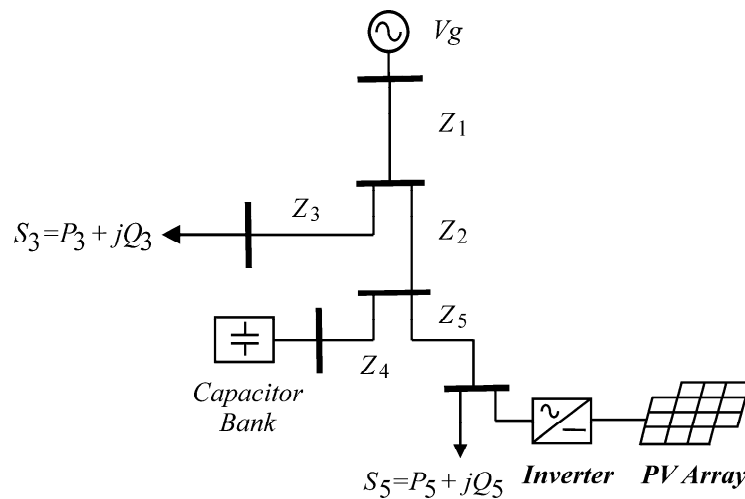


Figure 7. Microgrid supplied by a PV source.

The microgrid has a voltage source, a capacitor bank, five transmission lines, two linear loads, and the PV generation system. The dynamic operation of the system is represented by twelve DAEs. The voltage at the capacitors and the currents in the inductors where chosen as state variables. Figure 8 shows the equivalent circuit of the single-phase grid-connected PV generation system

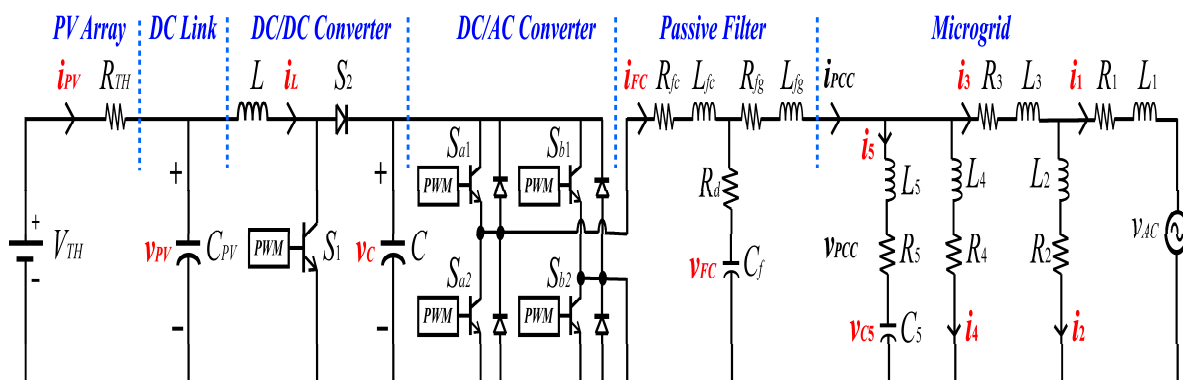


Figure 8. Equivalent circuit of the microgrid supplied by a PV source (state variables are highlighted in red).

The corresponding parameters are contained in Table 1. The PV array is solved for standard test conditions (STC), i.e., irradiance of  $1000 \text{ W/m}^2$  and temperature of  $25^\circ\text{C}$ . The PV system operates at the MPP.

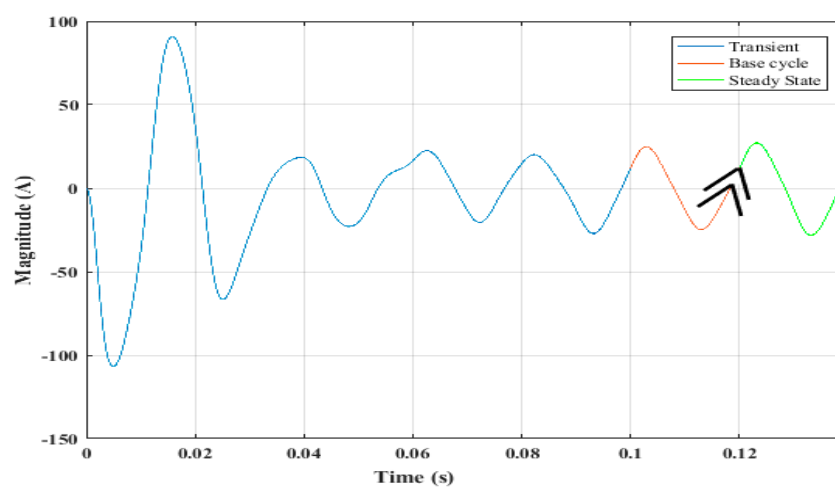
**Table 1.** Data of grid-connected PV generation system.

PV Array at STC		
$N_S$	17	Number of modules connected in series
$N_P$	2	Number of modules connected in parallel
$V_{oc}$	21.47 V	Open-circuit voltage per module
$I_{sc}$	7.6 A	Short-circuit current per module
$V_{mpp}$	17.1 V	Voltage at MPP per module
$I_{mpp}$	7.1 A	Current at MPP per module
$P_{max}$	121.41 W	Maximum power per module
$n_s$	28	Number of cells connected in series per module
$k_i$	$0.00502 \text{ A/}^\circ\text{C}$	Temperature correction factor for current
$k_v$	$-0.08 \text{ V/}^\circ\text{C}$	Temperature correction factor for voltage
$a$	1.3	Ideality factor of diode
Capacitor link		
$C_{PV}$	5500 F	Capacitance
DC/DC Converter		
$L$	9 mH	Inductance
$C$	2200 F	Capacitance
$F_s$	10 kHz	Switching Frequency
DC/AC Converter		
$f_s$	25 kHz	Switching Frequency
$m_a$	0.9	Modulation index
Filter		
$R_{fc}$	1 m	Resistance
$L_{fc}$	0.3 mH	Inductance
$R_{fg}$	1 m	Resistance
$L_{fg}$	0.15 mH	Inductance
$R_d$	2	Resistance
$C_f$	2.2 F	Capacitance
Microgrid		
$v_{AC}$	230 V	Voltage (rms)
$R_1$	1	Resistance
$R_2$	33	Resistance
$R_3$	1	Resistance
$R_4$	33	Resistance
$R_5$	1	Resistance
$L_1$	1 mH	Inductance
$L_2$	0.17 H	Inductance
$L_3$	1 mH	Inductance
$L_4$	0.17 H	Inductance
$L_5$	1 mH	Inductance
$C_5$	220 F	Capacitance

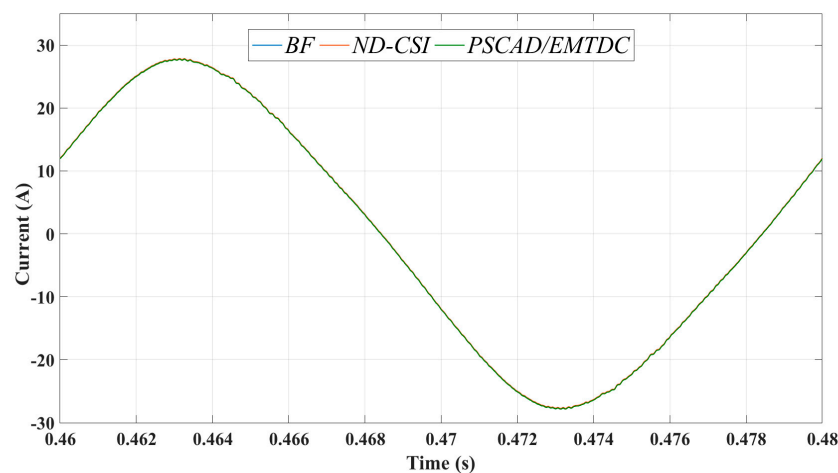
The resultant parameters of the PV array are obtained via the procedure described in Section 2.1 and presented in Table 2. Figure 9 shows the solution to the periodic steady state of the current waveform at PCC using the ND-CSI process. Five initial cycles and a base cycle were obtained before applying the ND method. One cycle of the periodic steady state solution is shown.

**Table 2.** Variables calculated for the PV generation system.

Key Points of V-I Curve of PV Array		
$V_{OC}$	365 V	Open-circuit voltage
$I_{SC}$	15.2 A	Short-circuit current
$V_{MPP}$	290.8 V	Voltage at MPP
$I_{MPP}$	14.2 A	Current at MPP
$P_{MAX}$	4129.4 W	Maximum power
Parameters for Thevenin Equivalent		
$R_S$	2.0 $\Omega$	Series resistance
$R_P$	2.172 k $\Omega$	Parallel resistance
$V_{TH}$	31.17 kV	Thevenin voltage
$R_{TH}$	2.174 k $\Omega$	Thevenin resistance

**Figure 9.** Current waveform at PCC.

In Figure 10, the results of the measured current waveform at the PCC obtained with the BF (using TR), ND-CSI, and PSCAD/EMTDC methods, respectively, are illustrated.

**Figure 10.** Periodic steady state current waveform at PCC.

The discrete periodic steady state current waveform is obtained with a reduced time step for the DN method. Then, it is reconstructed using CSI to obtain the final solution with a time step equal

to the used by the PSCAD/EMTDC simulator. An excellent agreement between responses can be observed. The corresponding comparison in harmonic content is shown in Figure 11. The order of the generated harmonics depends on the carrier frequency ( $f_{tri}$ ), and of the frequency modulation ratio ( $m_f$ ). Please notice that the harmonic distortion of the waveform is mainly due to the presence of third, fifth and seventh harmonics. The magnitude of the third harmonic is above the limit allowed by harmonic standards [34]. Again, a close agreement between the responses obtained with the BF, ND-CSI, and PSCAD/EMTDC are shown.

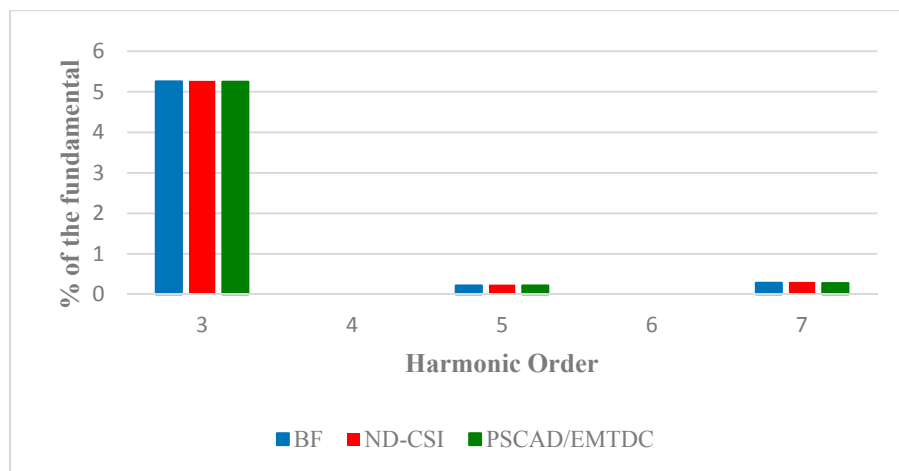


Figure 11. Harmonic content of current at PCC.

Table 3 shows the converged values of  $d$  and of the DC components (averages) of voltage and current at the PV array terminals.

Table 3. Simulation results of test case.

PV Array				
$V_{pv0}$	290.93	DC component of voltage at PV terminals		
$I_{pv0}$	14.20	DC component of current at PV terminals		
Boost converter				
$d$	0.277	Duty Ratio		
Point of common coupling				
$THD\ v_{PCC}$	BF 1.16%	PSCAD 1.16%	ND-CSI 1.17%	THD
$THD\ i_{PCC}$	5.27%	5.27%	5.29%	THD
$S$	4.7715 kVA	4.7715 kVA	4.7735 kVA	Apparent power
$P$	4.1350 kW	4.1350 kW	4.1370 kW	Active power
$PF$	0.8667	0.8667	0.8669	Power factor

Table 3 concludes that the obtained values agree with the MPP as given in Table 2. Also, Table 3 reports the THD and powers at the PCC obtained with the BF and ND-CSI methods, respectively. Please observe that the maximum error between responses is negligible, i.e., it is only 0.02% for the THD in  $i_{PCC}$ .

The algorithm used in this research was implemented with an AMD A8-6410 APU processor with AMD Radeon R5 Graphics, 2 GHz, and 6 GB of DDR3 on-board memory. Table 4 presents the variants of implementation of the ND method. In terms of the number of full time domain cycles (NFC) required for the convergence to the limit cycle, the BF method took 38 while the ND-CSI with  $\Phi$  variable took 18, and ND-CSI with  $\Phi$  constant took 30. However, the CPU time needed by the BF

method was 348 ms, the ND-CSI with  $\Phi$  variable method required 35 ms and the ND-CSI with  $\Phi$  constant needed 17 ms. In other words, the ND with  $\Phi$  constant is on average two times faster than the ND with  $\Phi$  variable. Also, the ND with  $\Phi$  constant is 20 times faster than BF method.

**Table 4.** Comparison of solution methods.

	BF	$\Phi$ Variable	$\Phi$ Constant
Time (ms)	348	35	17
NFC	38	18	30

### *Limitations of the Microgrid Modelling*

The ND method presents divergence when the microgrid or PV system parameters are erroneously determined.

An initial condition is required to execute the ND method; usually this condition is set to zero. The initial condition can be determined by using different methods, e.g., power flows solution. If the initial condition is not adequately estimated, the ND method may diverge or the time computer effort to converge may be considerable.

PV array parameters can change according to the environmental conditions making difficult to determine a new MPP. Moreover, the microgrid parameters may be recalculated to make the system stable.

The ND method may show difficulties towards convergence when the integration step is too large, i.e., when the number of samples is not sufficient to reconstruct the periodic steady state waveform. Furthermore, the CSI method presents a larger error when rebuilding the signal, taking more computational effort and time.

## **7. Conclusions**

An efficient and accurate time domain methodology to assess the harmonic distortion produced in microgrids with integration of PV sources has been proposed. The TD solution has been substantially enhanced with the combined application of extrapolation to the limit cycle based in the ND method and cubic splines interpolation to the voltage and current waveforms. The computational effort to obtain the time-domain solution has been dramatically reduced when compared against the BF approach, i.e. on average the ND-CSI with  $\Phi$  variable was 10 times faster than the conventional BF solution and 20 times faster with  $\Phi$  constant.

It is important to mention that the ND-CSI algorithm with  $\Phi$  variable needs of a simple modification to become the ND-CSI algorithm with  $\Phi$  constant. In addition, the ND-CSI approach with  $\Phi$  constant takes less computational effort than with  $\Phi$  variable. Therefore, it is worth doing this modification to the method.

The proposed ND-CSI methodology has been successfully verified against the solution obtained with the conventional BF solution and with the PSCAD/EMTDC simulator, respectively. A close agreement between the obtained responses has been achieved. For the reported case study, the maximum error between responses was 0.02%.

At this stage of research, the proposed ND-CSI methodology can be applied for the harmonic distortion assessment of microgrids with integrated photovoltaic sources. Moreover, it can be used for planning, operation and control of microgrids with PV generation sources. Research is under way to incorporate the combined effect of different renewable energy sources. Besides, the execution time of the proposed ND-CSI algorithm can be further reduced by using efficient computational techniques, such as parallel processing based on GPUs. Therefore, this may allow real time applications.

**Author Contributions:** M.D.-A. performed the simulation and modelling, analysed the data, and wrote the paper. A.M. analysed the results, reviewed the modelling and text, and supervised the related research work. R.C.-M. performed the modelling and analysed the extrapolation to the limit cycle method. A.R. provided critical comments and revised the paper.

**Funding:** This research received no external funding.

**Acknowledgments:** The first three authors gratefully acknowledge the Universidad Michoacana de San Nicolás de Hidalgo through the Facultad de Ingeniería Eléctrica, División de Estudios de Posgrado (FIE-DEP) Morelia, México, for the facilities granted to carry out this investigation. The first two authors acknowledge financial assistance from CONACYT to conduct this investigation.

**Conflicts of Interest:** The authors declare no conflict of interest.

## Nomenclature

### List of abbreviations

BC	Boost converter
BF	Brute force method
CSI	Cubic spline interpolation
DAE	Differential algebraic equations
EMTDC	Electromagnetic Transients including direct current
IGBT	Insulated Gate Bipolar Transistor
InC	Incremental conductance
MOSFET	Metal Oxide Semiconductor Field Effect Transistor
MPP	Maximum power point
MPPT	Maximum power point tracking
ND	Numerical differentiation method
ND-CSI	Numerical differentiation method combined with cubic spline interpolation
NFC	Number of full cycle
NR	Newton Raphson
PCC	Point of common coupling
PSCAD	Power systems computer aided design
PV	Photovoltaic
PWM	Pulse-width modulation
P&O	Perturb and observe method
RK4	Fourth-order Runge-Kutta
STC	Standard test conditions
TD	Time domain
TR	Trapezoidal rule
THD	Total harmonic distortion

### List of symbols

<b>C</b>	Iteration matrix
$f_0$	AC-system frequency
$f_{tri}$	Frequency of triangular carrier signal
<b>I</b>	Unit matrix
$I_{pv}$	Module PV generated current
$I_{PV}$	Array PV generated current
$I_o$	Module PV Saturation current
$I_0$	Array PV Saturation current
$m_f$	Frequency modulation ratio
$q$	Electron charge
$R_p$	Module PV equivalent parallel resistance
$R_s$	Module PV equivalent series resistance
$T$	Fundamental frequency period
$T_j$	Temperature on the p-n junction
$T_{on}$	BC switch is on state
$T_s$	BC Switching period

$v_{ac}$	Inverter output voltage magnitude
$v_{dc}$	Inverter input voltage
$v_{in}$	BC input voltage
$v_{out}$	BC output voltage
$V_{control}$	Positive sinusoidal signal control
$-V_{control}$	Negative sinusoidal signal control
$V_T$	Thermal voltage
$V_{tri}$	Triangular carrier waveform
$\mathbf{x}^i$	State vector at the beginning of the base cycle
$\mathbf{x}^{i+1}$	State vector at the end of the base cycle
$\Phi$	State transition matrix

## References

1. Eltawil, M.A.; Zhao, Z. Grid-connected photovoltaic power systems: Technical and potential problems. *Renew. Sustain. Energy Rev.* **2010**, *14*, 112–129. [\[CrossRef\]](#)
2. Kouro, S.; Leon, J.I.; Vinnikov, D.; Franquelo, L.G. Grid-connected photovoltaic systems: An overview of recent research and emerging PV converter technology. *IEEE Ind. Electron. Mag.* **2015**, *9*, 47–61. [\[CrossRef\]](#)
3. Ou, T.; Hong, C. Dynamic operation and control of microgrid hybrid power systems. *Energy* **2014**, *66*, 314–323. [\[CrossRef\]](#)
4. Kim, S.K.; Jeon, J.H.; Cho, C.H.; Kim, E.S.; Ahn, J.B. Modeling and simulation of a grid-connected PV generation system for electromagnetic transient analysis. *Sol. Energy* **2009**, *83*, 664–678. [\[CrossRef\]](#)
5. Barton, J.P.; Infield, D.G. Energy storage and its use with intermittent renewable energy. *IEEE Trans. Energy Convers.* **2004**, *19*, 441–448. [\[CrossRef\]](#)
6. Ou, T. A novel unsymmetrical faults analysis for microgrid distribution systems. *Int. J. Electr. Power Energy Syst.* **2012**, *43*, 1017–1024. [\[CrossRef\]](#)
7. Ou, T. Ground fault current analysis with a direct building algorithm for microgrid distribution. *Int. J. Electr. Power Energy Syst.* **2013**, *53*, 867–875. [\[CrossRef\]](#)
8. Ou, T.; Lu, K.; Huang, C. Improvement of transient stability in a hybrid power multi-system using a designed NIDC (Novel Intelligent Damping Controller). *Energies* **2017**, *10*, 488. [\[CrossRef\]](#)
9. Parker, T.S.; Chua, L.O. *Practical Numerical Algorithms for Chaotic Systems*, 3rd ed.; Springer-Verlag: New York, NY, USA, 1989.
10. Semlyen, A.; Medina, A. Computation of the periodic steady state in systems with nonlinear components using a hybrid time and frequency domain methodology. *IEEE Trans. Energy Convers.* **1995**, *10*, 1498–1504. [\[CrossRef\]](#)
11. Segundo, J.; Medina, A. Periodic steady state solution of electric systems including UPFCs by extrapolation to the limit cycle. *IEEE Trans. Power Deliv.* **2008**, *23*, 1506–1512. [\[CrossRef\]](#)
12. Morales Rodríguez, J. Modeling of Single-Phase Grid-Tied Photovoltaic Generation Systems in the Harmonic Domain. Master's Thesis, Centro de Investigación y de Estudios Avanzados del Instituto Politécnico Nacional, Unidad Guadalajara, Guadalajara, Jalisco, 2014.
13. Medina, A.; Segundo-Ramirez, J.; Ribeiro, P.; Xu, W.; Lian, K.L.; Chang, G.W.; Watson, N.R. Harmonic analysis in frequency and time domain. *IEEE Trans. Power Deliv.* **2013**, *28*, 1813–1821. [\[CrossRef\]](#)
14. Chapra, S.C.; Canale, R.P. *Numerical Methods for Engineers*, 6th ed.; Mc Graw-Hill: New York, NY, USA, 2009.
15. Burden, R.L.; Faires, J.D. *Numerical Analysis*, 9th ed.; Brooks-Cole Publishing: Boston, MA, USA, 2011.
16. Mehrasa, M.; Pouresmaeil, E.; Jorgensen, B.N.; Catalao, J.P.S. A control plan for the stable operation of microgrids during grid-connected and islanded modes. *Electr. Power Syst. Res.* **2015**, *129*, 10–22. [\[CrossRef\]](#)
17. Pouresmaeil, E.; Jorgensen, B.N.; Mehrasa, M.; Erdinc, O.; Catalao, J.P.S. A Control Algorithm for the Stable Operation of Interfaced Converters in Microgrid Systems. In Proceedings of the IEEE PES Innovative Smart Grid Technologies Europe (ISGT Europe), Istanbul, Turkey, 12–15 October 2014.
18. Agundis-Tinajero, G.; Segundo-Ramirez, J.; Peña-Gallardo, R.; Visairo-Cruz, N.; Nuñez-Gutierrez, C.; Guerrero, J.M.; Savaghebi, M. Harmonic Issues Assessment on PWM VSC-Based Controlled Microgrids Using Newton Methods. *IEEE Trans. Smart Grid* **2018**, *9*, 1002–1011. [\[CrossRef\]](#)



19. Ivry, P.M. Predicting Stochastic Harmonics of Multiple Converters in a Power System (Microgrid). Ph.D. Thesis, University of Nottingham, Nottingham, UK, 2016.
20. Hren, A.; Mihalic, F. An improved SPWM-based control with over-modulation strategy of the third harmonic elimination for a single-phase inverter. *Energies* **2018**, *11*, 881. [[CrossRef](#)]
21. Pouresmaeil, E.; Mehrasa, M.; Shokridehaki, M.A.; Rodrigues, E.M.G.; Catalao, J.P.S. Stable operation of distributed generation units in microgrids networks. In Proceedings of the 2015 Australasian Universities Power Engineering Conference (AUPEC), Wollongong, Australia, 27–30 September 2015.
22. Ou, T.; Hong, C.; Lu, K. Development of intelligent MPPT (maximum power point tracking) control for a gridconnected hybrid power generation system. *Energy* **2013**, *50*, 270–279.
23. Castañer, L.; Silvestre, S. *Modelling Photovoltaic Systems Using PSpice*, 1st ed.; John Wiley & Sons: Chichester, UK, 2002.
24. Rauschenbach, H.S. *Solar Cell Array Design Handbook*, 1st ed.; Litton Educational Publishing: New York, NY, USA, 1980.
25. Kalogirou, S.A. *Solar Energy Engineering*, 2nd ed.; Elsevier Academic Press: London, UK, 2013.
26. Villalva, M.G.; Gazoli, J.R.; Filho, E.R. Comprehensive approach to modeling and simulation of photovoltaic arrays. *IEEE Trans. Power Electron.* **2009**, *24*, 1198–1208. [[CrossRef](#)]
27. Liserre, R.; Teodorescu, R.; Blaabjerg, F. Sitability of photovoltaic and wind turbine grid connected inverters for a large set of grid impedance values. *IEEE Trans. Power Electron.* **2006**, *21*, 263–272. [[CrossRef](#)]
28. Mohan, N.; Underland, T.M.; Robbins, W.P. *Power Electronics: Converters, Applications, and Design*, 3rd ed.; John Wiley & Sons: Hoboken, NJ, USA, 2003.
29. Luo, F.L.; Ye, H. *Advanced DC/DC Converters*, 2nd ed.; CRC Press: Boca Raton, FL, USA, 2016.
30. Rashid, M.H. *Power Electronics Handbook*, 4th ed.; Elsevier: Cambridge, MA, USA, 2018.
31. Balagurusamy, E. *Numerical Methods*, 1st ed.; Mc Graw Hill: New Delhi, India, 1999.
32. Medina, A.; Garcia, N. Fast time domain computation of the periodic steady-state of systems with nonlinear and time-varying components. *Int. J. Electr. Power Energy Syst.* **2004**, *26*, 637–643. [[CrossRef](#)]
33. Cheney, W.; Kincaid, D. *Numerical Mathematics and Computing*, 6th ed.; Brooks/Cole: Monterey, CA, USA, 2008.
34. IEEE Standard. *IEEE Recommended Practices and Requirements for Harmonic Control in electrical Power Systems*; IEEE Standard 519-1992; IEEE: New York, NY, USA, 1993.



© 2018 by the authors. Licensee MDPI, Basel, Switzerland. This article is an open access article distributed under the terms and conditions of the Creative Commons Attribution (CC BY) license (<http://creativecommons.org/licenses/by/4.0/>).